Visualization methods for heat transport in Miami Isopycnic Circulation Ocean Model (MICOM)

Ramprasad Balasubramanian & Vishal Shah
Department of Computer and Information Science
University of Massachusetts Dartmouth
No. Dartmouth, MA - 02343
rbalasubrama@umassd.edu

Amit Tandon
Department of Physics
University of Massachusetts Dartmouth
No. Dartmouth, MA - 02343
atandon@umassd.edu

Abstract

In this paper we propose visualization approaches inspired by physical metrics for measuring heat transport in ocean data. We propose metrics that have physical significance in the context of Physical Oceanography. We propose methods to visualize the heat index (a metric we define that looks at heat transport at individual latitude-longitude points that combine temperature, depth and velocity). Plotting the heat indices provides the range of latitudes and longitudes where there is significant activity (defined later). These regions are visualized using vector fields and other visualization techniques. The enormous amount of data generated by MICOM can be considerably reduced for the purpose of climate diagnostics, using this approach. The model is demonstrated on data from several days and different layers of the Atlantic ocean.

1. Introduction

Due to enormity of the high-resolution ocean data, computation is expensive both in terms of computing power and time (on top of the added space complexity to this problem). This leads to use of the low-resolution data for quick understanding of the system behavior. While the low-resolution data is considerably smaller in quantity, it also lacks the quality of information ordinarily available in the high-resolution data. In this work we take two metrics in Physical Oceanography, Poleward heatflux and Eastward heatflux. The heatfluxes provide a measure of the heat transport poleward and eastward for each latitude and longitude respectively. While this is a very important metric, it is difficult to visualize, as it produces a graph as seen in Figure 1. In order to better visualize the heat transport we break the metrics down to their fundamental components to define new metrics.

As in most large datasets of this nature, there is a great deal of redundancy. In this paper we wish to take advantage of this redundancy, by identifying the regions of redundancy and imposing conditions of low-resolution and imposing high-resolution condition in the case of low-redundancy. To recognize these regions we will identify and define metrics that can be applied in a wide-range of applications.

In this paper we specifically propose the use of this method to identify the regions of activity using the Poleward and Eastward heat transport. We would like to be able to identify and isolate mesoscale coherent structure like jets and eddies. The rest of the paper is organized as follows - the introduction is followed by previous work in this area, then a brief introduction to the dataset is provided, followed by the derivation of the metric used in this study, the next section addresses the method and algorithm used in this work, followed by results and conclusions.

2. Previous Work

This section highlights only some of the research that focused on data refinement and visualization methods for oceanic datasets, and is not meant to be a comprehensive review.

Finding the appropriate method or suite of methods to best portray the meaning of the given data is a challenge. [7]. Prior to the availability of advanced visualization techniques, ocean model outputs were visualized in 2D rectangular flat surfaces. In order to render such output more realistically, various techniques have emerged. These included digital elevation models, wire frame overlays, and grayscale and color-shading mapping techniques [13]. A tool called Oceanographic Visualization Interactive Research Tool (OVIRT) has been developed to explore the utility of scalar field volume rendering in visualizing environmental ocean data and to extend some of the classical 2D oceanographic displays into a 3D visualization environment [11].

In order to analyze the large scientific datasets, data management techniques are often used to identify areas of interest within the dataset. This allows the reduction of a dataset size and dimensionality, and the estimation of missing val-

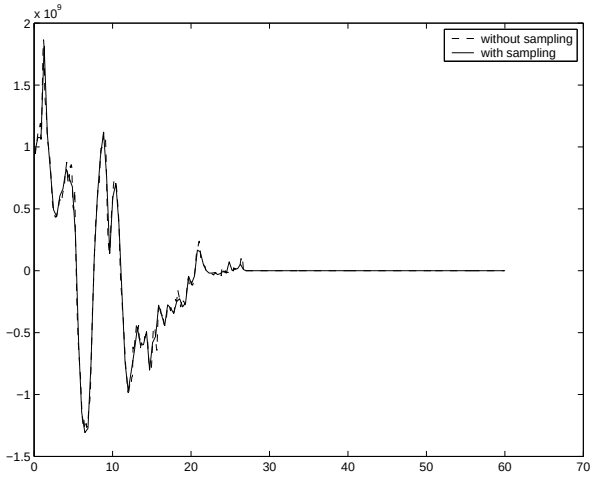

Figure 1: Poleward Heat Flux for Day 3, Layer 2.

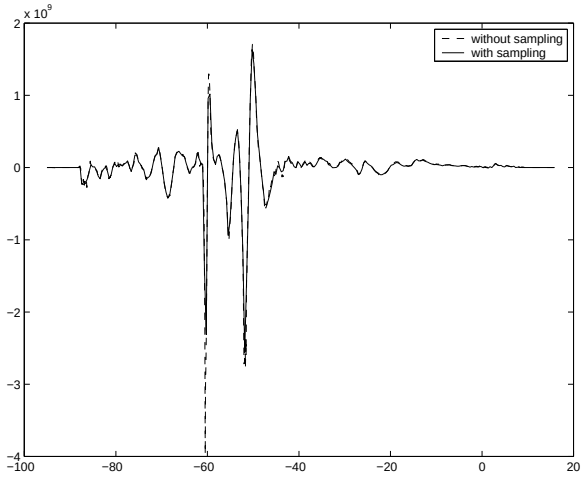

Figure 2: Eastward Heat Flux for Day 3, Layer 2.

ues or correction of erroneous entries [9]. In this study, to deal with those large scientific datasets, a two-step approach was proposed: (1) Using data mining algorithms to identify areas of interest within the dataset. (2) Using visualization techniques based on perceptual cues to display the results of the data mining step [10]. A greater understanding of a data set and reduced analysis time, supplementing traditional methods with 3D visualization and novel display techniques have also been proposed [8]. Visualization techniques used for ocean data have included - trivariate (B-Splines) parametric representation of data [15], feature-extraction and tracking [17], feature based visualization for tracking sea surface temperature [16], and measurement and analysis of feature velocities (usually referred to as estimation of optic flow) [3]. Since the ocean model is highly nonrigid (known as fluid data in motion classification), relaxation methods have been proposed, by dropping the constraints imposed by the fluid motion [6].

In applications such as oceanography visualization, one concern is obtaining good-enough models from real data due to their enormity. The proposed methods could prove very useful in distilling the enormous amount of information into one that is sufficient for this application by detecting regions of interest and regions of non-interest (little or no observable change, based on the defined metrics). While most of these works have performed sub-sampling in some fashion, the significance of our work lies in defining standardized metrics to measure the loss (or gain) of information due to the sub-sampling, relating to the physical characteristics of the variable being visualized. Since modification to one variable may have a marked change in other variables, this work would be important to both oceanographers and computer scientists.

3. Numerical General Circulation Model: MICOM

MICOM is the Miami isopycnic ocean circulation model. This numerical model has its origins in the seminal work done by [4], which uses density as a vertical coordinate for the ocean. In this model, the data is saved at different spatial and temporal (i.e. varying depth) locations in the ocean. Typically the data is collected daily (or every three days) for 6 or 12 months at a time. Each data set has multiple variables associated with them, such as velocity, temperature, salinity etc. The data usually is available in two resolutions The high-resolution data is usually $\frac{1}{12}^o$ longitude by $\frac{1}{12}^o$ latitude by 35 layers. The finest resolution studies contrast strongly with the low resolution and show particularly turbulent behavior [12].

3.1. Physical Diagnostic Metric - I: The Poleward heat flux and the Eastward heat flux

Measurements done to-date (e.g. [1] for the Pacific Ocean, [2] for the Atlantic) have suggested that the mesoscale eddies and mesoscale features play a strong role in carrying heat poleward. MICOM is one of a few suite of models, where the resolution of the numerical experiments is high enough to resolve the mesoscale eddies. Hence a question alluded to before arises, i.e, to what spatial extent must we resolve the features to get an accurate description of the poleward heat flux in individual isopycnal layers? In addition, how can the physical metric of Poleward heat flux and Eastward heat flux be used to visualize the ocean data better? This connects to our previous concepts of interesting and non-interesting regions.

In accordance with the usual oceanographic notation, we take x to be the Eastward and y to be the Northward direc-

tion. Poleward heat flux in an isopycnal layer l of thickness dp(x,y,l)can be defined as

$$P(y,l) = \int_{x_W}^{x_E} \rho C_p v(x,y,l) T(x,y,l) dp(x,y,l) dx \quad (1)$$

where, x_W is the western boundary of the Ocean basin (the American continent for our North Atlantic simulations), x_E is the eastern boundary of the ocean basin, ρ is the density of the seawater, C_p is the specific heat, v is the meridional velocity component (in the Northward direction - positive values, in the Southward direction - negative values), and T the temperature at points (x, y) for layer l. While the Cartesian formulae are presented here for simplicity, the integral evaluations are done using the full spherical geometry equivalent of the above formulae, that is, $dx = Rcos(\phi)d\zeta$, where $d\zeta$ is the range in longitude, R is the radius of the Earth, and ϕ the latitude. Similarly the eastward heat flux is defined as

$$E(x,l) = \int_{y_S}^{y_N} \rho C_p u(x,y,l) T(x,y,l) dp(x,y,l) dx \quad (2)$$

In our analysis that follows, we scale the poleward and eastward heat fluxes by the factor ρC_p, since we are mainly interested in identifying regions of interest based on these physical metrics and testing the convergence to these metrics at different resolutions. These two quantities are taken as the physical metrics which will be useful to visualize areas of interest.

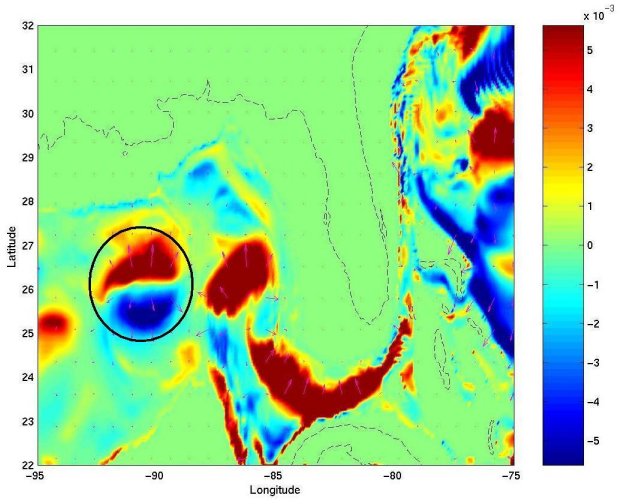

Figure 3: An eddie in the Gulf of Mexico (day 6, layer 6).

3.2. Physical Diagnostic Metric - II: The Poleward heat flux and the Eastward heat flux

While the Poleward and Eastward heat fluxes are a good measure of heat transport in the Northern (and Southern) and Eastern (and Western) directions we deemed them insufficient for visualizing individual quandrants (for a specific latitude-longitude regions) for the following reasons. The heat flux represents a cummulative sum (in the discrete case) for individual latitude and longitude, i.e., it provides a single value per latitude or longitude. This provides no sense of the heat transport at different areas of the same latitude or longitude. As the values at each point can be positive or negative (due to change in direction of flow), using the sum only can be misleading. Due to this variation we defined two new metrics that would enable us to view the individual latitude-longitude points.

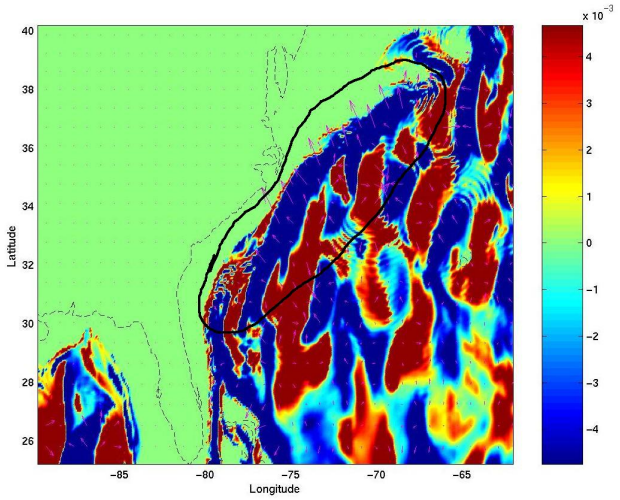

Figure 4: A jet stream (day 6, layer 6).

We defined our first metric, called the *heat content* as the product of the velocity, temperature and depth for each layer, as given by the following equation for the Poleward flow:

$$heat\_content(i,j,l) = v(i,j,l) * t(i,j,l) * dp(i,j,l) \quad (3)$$

where *i* spans the range of the latitude and *j* spans the range of the longitude and *l* is the layer. A similar metric is defined for the Eastward flow using *u(i,j)* instead of *v(i,j)*.

This provides us with individual heat content at every point in the quadrant. This metric by itself is insufficient as there is no correlation to the heat flux, the overall heat transport per latitude or longitude. Hence we define our second metric - the heat index. The poleward heat index is defined as follows:

$$heat\_index(i,j,l) = \frac{v(i,j,l) * t(i,j,l) * dp(i,j,l)}{P(i,l)} \quad (4)$$

where , *i and j* are the same as before. *P(i,l)* is as defined in (1). A similar metric is defined for the Eastward heat index with *u(i,j,l)* replacing *v(i,j,l)* and *E(j,l)* replacing *P(i,l)*.

This would still face the limitation of summation of negative and positive values in the heat flux. In order to isolate the Northward (and Southward) and Eastward (and Westward) heat transfers, we refined Eqn. (4) to:

$$heat\_index\_Northward(i,j) = \frac{heat\_index^{+}(i,j)}{P^{+}(i,l)} \quad (5)$$

$$heat\_index\_Southward(i,j) = \frac{heat\_index^{-}(i,j)}{P^{-}(i,l)} \quad (6)$$

where $heat\_index^{+}(i,j)$ represents all the positive values (Poleward direction) and $heat\_index^{-}(i,j)$ represents all the negative values (Southward direction). Similarly by replacing *v(i,j,l)* by *u(i,j,l)* we can get the Eastward and Westward directional flows. So by computing the heat indexes based on direction we can visualize the Poleward and Eastward heat transfers better.

4. Results

4.1 Dataset

The data was obtained from National Center for Atmospheric Research (NCAR). High resolution ocean data can run into several terabytes. It is impractical and expensive to use the entire dataset for the explicit purpose of desktop visualization. We have confined our attention to the Atlantic Ocean (from latitude 13.78^o - 66.26^o, longitude $-95.04^o - 16^o$). The high resolution data is available every 0.08^{th} of degree along the longitude and approximately about 0.055^{th} of a degree in the latitude. This corresponds to grid of 1389 points along the longitude by 944 points along the latitude. Measurements are available for 35 layers (only 8 are used in this experiment), for each layer, we use 4 variables, namely depth of the layer(also known as layer thickness), temperature, U baroclinic (eastward) velocity component and V baroclinic (northward) velocity component, for each point on the grid. After converting from its native format to a matrix of longitude, latitude, depth, temperature and U-V velocity components the Poleward and Eastward heat flux are computed, using equations (1) and (2) respectively for each layer. Figures 1 and 2 show the Poleward and Eastward heat flux respectively, for day 3 (of the dataset), layer 2. The horizontal axis corresponds to longitude (latitude) and the vertical axis corresponds to the Poleward (Eastward) heat flux.

4.2 Mesoscale Structure Identification Algorithm

One of the primary goals of this work was to enable detection of mesoscale structres in the ocean using the heat transport as a metric. Mesoscale structures can vary from

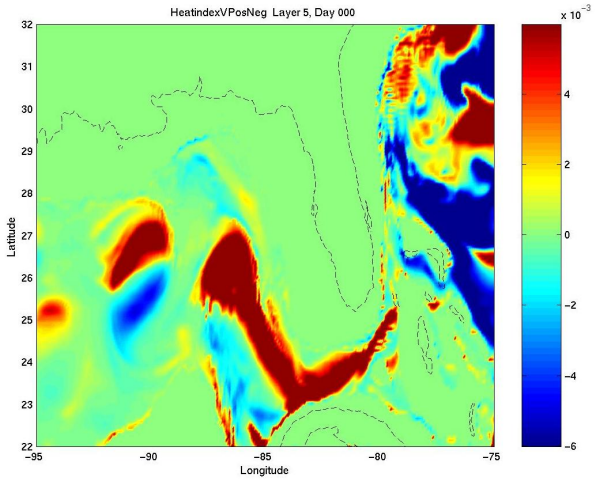

Figure 5: Eddie on Day 0 Layer 5

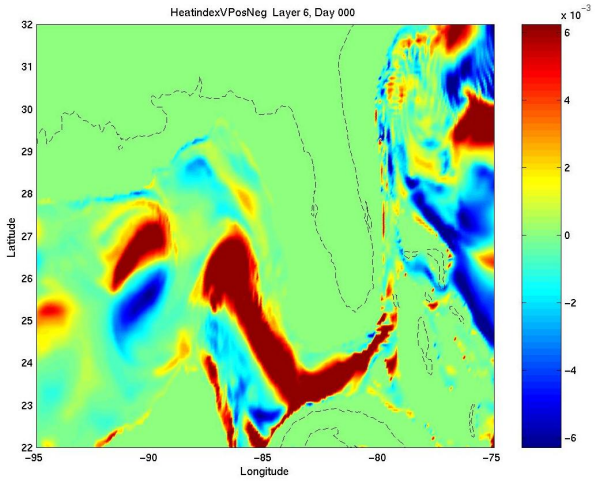

Figure 6: Eddie on Day 0 Layer 6

eddies to meandering currents to jets to vertical compression of strong convergence and divergence. Eddies, dynamically arise from baroclinic instability, that have a strong rotational component [14]. The rotational component (or dominant radius) can vary between 10 to 100 kilometers. They also tend to be large in radii, closer to the equator, than poleward. Meandering currents tend to move in various directions in short intervals. Areas of vertical compression of strong convergence and divergence can be observed as points (or locations) about which there is strong convergence or divergence, and can be observed in several layers. Jets are strong unidirectional currents, that typically transport heat.

To identify these regions we need to detect mesoscale structures and be able to isolate the latitude and the longitude, of such activities. In our approach, we exploit the

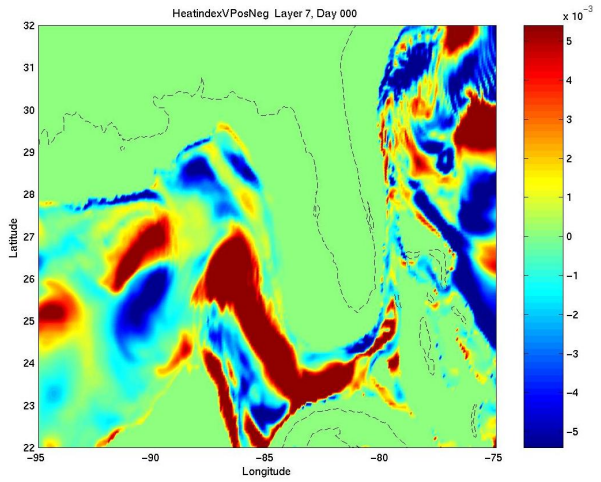

Figure 7: Eddie on Day 0 Layer 7

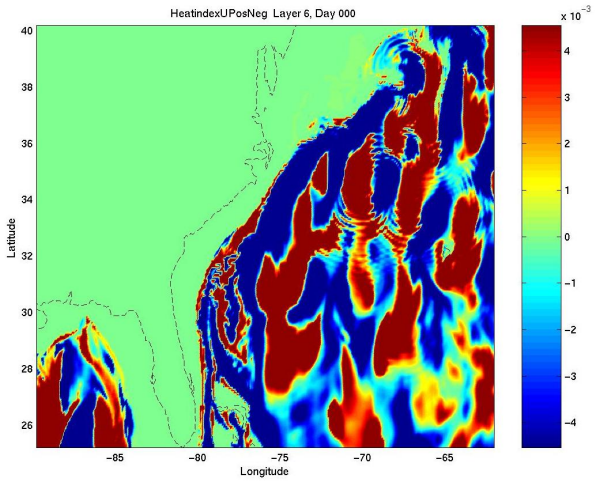

Figure 8: Gulf Stream layer 6 day 0

properties of these structures with the visualization of our metrics. Since our metrics would enable us view the flow of heat in each individual direction we would expect an eddie to be show up as a structure that has flow in all four directions. Similarly a jet would appear as a long unidirectional flow.

4.3 Visualization

An example of an eddie is shown in Figure (3). For better understanding the flow field of the velocity vectors are also plotted. The vector fields validate the directional correctness of our metric. The blue color indicates regions of southern transport and red indicates regions of northern transport. A similar example of a jet is should in Figure (4). Here blue represents regions of western transport and red indicates regions of eastern transport. As the heat index combines the layer thickness, temperature and velocity components, we chose to ignore the surface layer (layer 1) for the simple reason that this layer is subject strong atmospheric influences. We focused only on layers 2 through 8. Applying the methods described in the previous subsections, we can isolated regions of activity and inactivity. Regions of inactivity would simply appear with NULL values (same as the land regions). Visualizing additional layers for the same range of latitudes and longitudes show that the activities continue through several layers, as can be seen in layers 5 (Figure 5), 6 (Figure 6) and 7 (Figure 7). In this particular example we track the eddie through the various layers till it weakens. Similarly we track the gulf stream (a well known phenomenon, that transports heat poleward along the east coast of the United States) across several days, keeping the layer fixed. Figures 8, 9 and 10 show this jet for layer 6 for days 0, 3 and 6. The continuous curve indicates coastline.

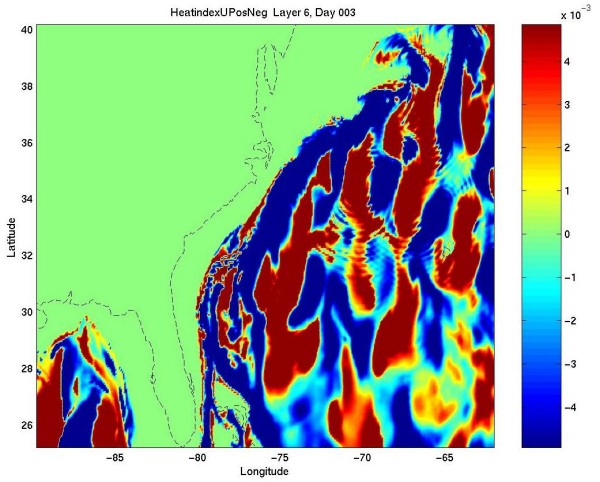

Figure 9: Gulf Stream layer 6 day 3

5. Summary and Conclusions

In this paper we propose new metrics that prove to be very effective is visualizing heat transport in the MICOM ocean model. We demonstrate the effectiveness of this approach in identifying key mesoscale structures such as jets and eddies. This paper we also present a robust approach to identifying regions of interest and non-interest through simple examination of the metrics that we have defined. The approach can be extended to study other metrics such as momentum flux and to study temperature structures and salinity structures.

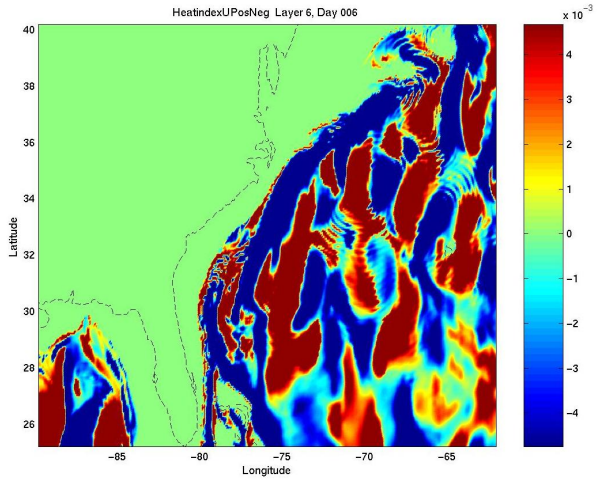

Figure 10: Gulf Stream layer 6 day 6

References

[1] D. Roemmich, J. Gilson and B. Cornuelle, "Mean and time-varying meridional trsnport of heat at the tropical/subtropical boundary of the North Pacific Ocean," *Journal of Geophysical Research-Oceans*, Vol. 106, pp8957-8970, 2001.

[2] H. L. Bryden, " Oceanic heat transport across 24°N latitude," *Interaction Between Global Climate Subsystems: The legacy of Hann. Eds.: G.A. McBean and M Hantel, Geophysical Monographs*, Vol. 75, pp65-75, 1993.

[3] Barron, J. L., Flect, D. J., Beauchemin, S. S.," Performance of Optic Flow techniques." *Proceedings of IEEE CVPR'92*, 236-242, June 1992.

[4] Bleck, R., Boudra, D., "Initial testing of a numerical ocean circulation model using a hybrid (quasi iospycnic) vertical coordinate." *Journal of Physical Oceanography*, 11, 755-770, 1981.

[5] Bryan, K. Poleward heat transport in the ocean. A review of a hierarchy of models of increasing resolution. Tellus, 43AB, 104-115, 1991.

[6] Cohen, I., Herlin. A motion computation and interpretation framework for oceanography satellite images. SCV 95, 13-18, 1995.

[7] Gaither, K., Moorhead - II, R. J. Visualizing vector information in ocean environments. 'Challenges of Our Changing Global Environment'. Conference Proceedings. OCEANS '95 MTS/IEEE IEEE, New York, NY, USA; vol.3 1907-14, 1995.

[8] Head, M. E. M., Phu-Luong, Costolo, J. H., Countryman, K., Szczechowski, C. Applications of 3-D visualizations of oceanographic data bases. Oceans '97. MTS/IEEE. Conference Proceedings. IEEE, New York, NY, USA; vol.2 1510, 1997.

[9] Healey, C. G. Building a perceptual visualization architecture. Behavior-and Information-Technology. vol.19, no.5 349-66, Sept.-Oct. 2000.

[10] Healey, C. G. On the use of perceptual cues and data mining for effective visualization of scientific datasets. Proceedings Graphics Interface '98. Canadian Inf. Process. Soc, Toronto, Ont., Canada; 177-84, 1998.

[11] Moorhead - II, R. J., Everitt, C., Jones, S., McAllister, J., Barlow, J. Oceanographic Visualization Interactive Research Tool (OVIRT). Proceedings-of-the-SPIE -The-International-Society-for-Optical-Engineering. 2178, 24-30, 1994.

[12] Paiva, A. M., Hargrove, J. T., Chassignet, E. P., Bleck, R. Turbulent behavior of a fine mesh (1/12) numerical simulation of the North Atlantic. J. Mar. Sys., 21, 307-320, 1999.

[13] Rochon, G. L., Luong, P. V., Costolo, J. H., Ruby, G., Goon, L. A. Three dimensional visualization of oceanographic data: a case study of the Gulf of Mexico's coastal interface with Texas and Louisiana. Oceans '97. MTS/IEEE. Conference Proceedings IEEE, New York, NY, USA; vol.2 1510, 1997.

[14] Tandon, A., Garrett, C. On a recent parameterization of mesoscale eddies. Journal of Physical Oceanography, 26, 406-411, 1996.

[15] Tuohy, S. T., Yoon, J. W., Patrikalakis, N. M. Trivariate parametric B-splines for visualization of ocean data. Conference Proceedings. OCEANS '95 MTS/IEEE IEEE, New York, NY, USA; vol.3 1601-8, 1995.

[16] Yang, Q., Parvin, B. Feature Based Visualization of Geophysical Data. Proceedings of the IEEE International Conference of Computer Vision and Pattern Recognition (CVPR), June 2000, 276-281.

[17] Zhu, Z., Moorhead - II, R. J., Anand, H., Raju, L. R. Feature extraction and tracking in oceanographic visualization. Proceedings-of-the SPIE -The-International-Society-for-Optical-Engineering. 2178, 31-39, 1994